Materials Research. 2019; 22(suppl. 2): e20180640
DOI: http://dx.doi.org/10.1590/1980-5373-MR-2018-0640

Nanoporous Pd with Tunable Pore Size prepared by Dealloying $Pd_{30}Cu_{40}Ni_{10}P_{20}$ Metallic Glass and Their Catalytic Performance

Kui Zhu[a], Zhi Yang[a], Xuhai Zhang[a], Shencheng Yang[a,b], Yuqiao Zeng[a]*, Jianqing Jiang[a,c]

[a] *Jiangsu Key Laboratory of Advanced Metallic Materials, School of Materials Science and Engineering, Southeast University, Nanjing, 211189, China*
[b] *Huzhou University, huzhou, 313000, China*
[c] *Nanjing Forestry University, Nanjing, 210037, China*

Received: September 25, 2018; Revised: April 11, 2019; Accepted: April 30, 2019

This work reports the formation of nanoprous Pd with tunable pore size and high stability by dealloying $Pd_{30}Cu_{40}Ni_{10}P_{20}$ metallic glass. The results show that lower dealloying temperature results in smaller pore size while the dealloying duration does not cause distinct change in the porous structure, even at an ambient dealloying temperature. The glassy structure and the multiple components in the precursor alloy are attributed to the hindered diffusion of Pd atoms and a slow coarsening rate of the nanoprous structure. The fully dealloyed porous sample with the smallest average pores size of 10 nm exhibit much higher catalytic activity when compare with the commercial Pd/C catalysts while the specimen with an average pores size of 13 nm shows the highest catalytic stability among the fully dealloyed alloys.

Keywords: *Metallic glass, dealloying, nanoporous, coarsen, catalyst.*

1. Introduction

Recently, nanoporous metals have received considerable attention due to their unique morphological structure and chemical properties which can be widely applied in electrochemical catalysis, sensor, optics and bioinstrumentation [1-4]. Dealloying technique is one of the most efficient approaches to fabricate nanoporous metals [5,6]. During dealloying, the electrochemically more active elements are selectively leached by electrolyte and the more noble elements will diffuse through an up-hill way to form three-dimensional continuous ligaments, leaving behind a highly porous structure[7]. To achieve a uniform nanoporous structure, the dealloying precursor should contain a homogenous structure at nanoscale. Usually, binary solid solutions and intermetallic alloys, such as Au-Ag, Au-Cu and Cu-Mn, are one of these ideal dealloying precursors [8-12]. Recently, there are some attempts to synthesize nanoporous metals by dealloying metallic glasses. When compared with the conventional solid solution or intermetallic precursors, metallic glasses have several advantages. Firstly, more than thousands of metallic glass systems have been developed, providing the nanoporous metals numerous dealloying precursors [13-15]. Till now, several nanoporous metals, such as Cu, Pt and nanoporous Au, were obtained by dealloying different metallic glasses [16-18]. Secondly and more importantly, most of the metallic glasses are composed of more than three kinds of elements, making it possible to form multicomponent nanoporous metals with higher catalytic activity, structure stability and etc. For instance, nanoporous PdNi had been prepared by dealloying $Pd_{30}Ni_{50}P_{20}$ metallic glass[19]. Nanoporous AuPd was fabricated by dealloying Au-based metallic glass. Doping effect (doping Pd with Au) highly improved the structure stability of nanoporous Au[20].

In this work, we tried to fabricate new nanoporous metals with both high catalytic activity and structure stability through doping. It has been shown by former research work that Ni can improve the catalytic activity of Pd[19,21], while Cu is beneficial for stabilize nanoporous structure[22]. Therefore, the $Pd_{30}Cu_{40}Ni_{10}P_{20}$ metallic glass was chosen as the precursor alloy. Both dealloying temperature and duration were varied to tune the chemical composition and microstructure of the multicompositional nanoporous alloy. And the catalytic performance of the nanoporous alloys towards the formic acid oxidation was studied.

2. Experimental Methods

The $Pd_{20}Cu_{40}Ni_{10}P_{20}$ alloy was prepared by melting a pre-alloyed Pd-Ni-P ingot with Pd, Ni, Cu metals. The purity of the metals used in this study is higher than 99.99%. After a repeating B_2O_3 flux treatment[23], the $Pd_{20}Cu_{40}Ni_{10}P_{20}$ alloy was remelted and subjected to melting-sputtering in an argon atmosphere. The as-spun ribbons were about 2 μm in thickness and 2 mm in width. The glassy structure of the ribbons was confirmed by X-ray diffraction (XRD) using Cu Kα radiation and a differential scanning calorimeter (DCS). The electrochemically properties of the ribbons was evaluated by a potentiodynamic polarization test.

The glassy $Pd_{30}Cu_{40}Ni_{10}P_{20}$ alloy was potentiostatically dealloyed at 0 ºC, 25 ºC and 50ºC in a mixed solution of 0.8mol/L H_2SO_4 and 0.2mol/L H_3PO_4 for different duration.

*e-mail: zyuqiao@seu.edu.cn.

The chemical compositions of the dealloyed samples were characterized by energy dispersive X-ray spectrometer (EDS) and the surface morphology was observed using scanning electron microscopy (SEM, FEI. Sirion 200). The electrochemical properties of the dealloyed sample for formic acid electro-oxidation were evaluated in a standard three-electrode electrochemical cell in CHI 760D electrochemical workstation, where the porous samples were used as the working electrode, a Pt foil was used as a counter electrode and a mercury sulfate electrode (MSE) was used as the reference electrode.

3. Results and Discussion

3.1 Formation of Pd30Cu40Ni10P20 metallic glass

Figure 1 shows the XRD pattern of the as-spun $Pd_{30}Cu_{40}Ni_{10}P_{20}$ ribbon. There is a broad diffraction hump centering at 2θ of 42.2º. No sharp peaks corresponding to crystalline structure can be seen, indicating the formation of a uniform amorphous structure. The inset of Figure 1 is the DSC curve taken at a heating rate of 0.67 K/s. It can be seen that the as-spun sample exhibits an endothermic peak due to the glass transition, followed by a supercooled liquid region and then several exothermic peaks due to the crystallization. The glass transition behavior further confirms the glassy state of the as-spun $Pd_{30}Cu_{40}Ni_{10}P_{20}$ ribbons.

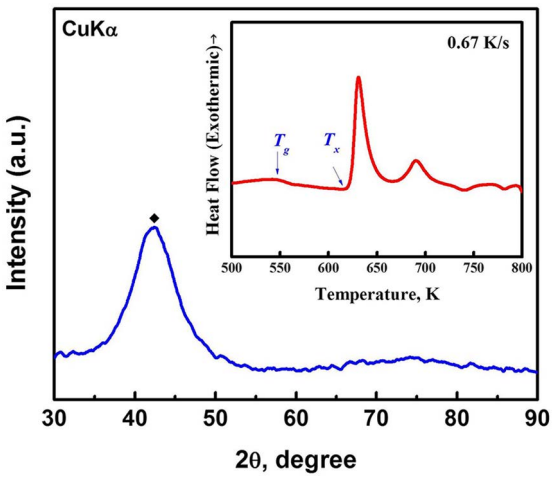

Figure 1. XRD pattern of the as-spun $Pd_{30}Cu_{40}Ni_{10}P_{20}$ metallic glass, the inset is the DSC curve of the as-spun $Pd_{30}Cu_{40}Ni_{10}P_{20}$

3.2 Dealloying Pd30Cu40Ni10P20 metallic glass

The inset of Figure 2 displays the Tafel curve of the as-spun $Pd_{20}Cu_{40}Ni_{10}P_{20}$ alloy measured in 0.8 mol/L H_2SO_4 + 0.2 mol/L H_3PO_4 solution at 25 ºC at a scanning rate of 0.2 mV/s. The dramatic decreasing current density along with the increasing applied voltage (-700 mV~ 750 mV *vs* SCE) is corresponding to cathodic reactions, while the anodic region is in 750 mV～100 mV *vs* SCE where no passivation behavior is observed. The applied dealloying potential of $Pd_{30}Cu_{40}Ni_{10}P_{20}$ was selected at 820 mV *vs* SCE. Figure 2 is the current *vs* time curve of the potentiostatically dealloyed $Pd_{30}Cu_{40}Ni_{10}P_{20}$ glass. The dealloying process can be divided into three different current stages, similar to that of dealloying solid solutions and intermetallic metals: initial rising stage (0~600 s) where leaching Ni, Cu and P from the glass is the dominant process, steady stage (600~5400 s) where leaching reactions and coarsening maintain a dynamic balance and fast dropping stage (5400-7200s) where leaching finishes and coarsening becomes the dominant process [24].

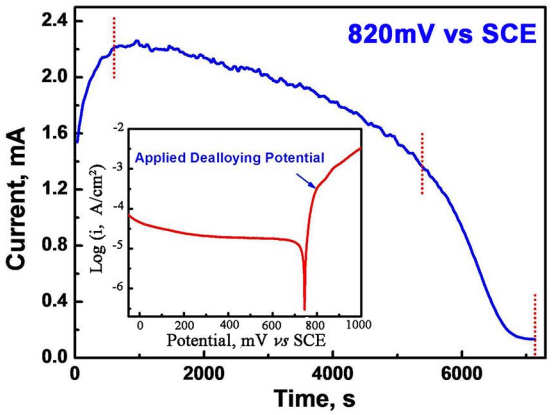

Figure 2. Current *vs* time curve of the potentiostatically dealloyed $Pd_{30}Cu_{40}Ni_{10}P_{20}$ glass, the inset is the Tafel curve of the as-spun $Pd_{20}Cu_{40}Ni_{10}P_{20}$ alloy measured in 0.8 mol/L H_2SO_4 + 0.2 mol/L H_3PO_4 solution at 25 ºC at a scanning rate of 0.2 mV/s

EDS analysis was performed on the samples dealloyed for 600 s, 1800 s and 7200 s at 25 ºC. The data were summarized in Table 1. It can be seen that with the increasing dealloying duration, the atomic content of Pd increases while those of Cu, Ni and P decrease. It is reasonable since Cu, Ni and P elements have much higher electrochemical activity when compared with Pd.

Table 1. Chemical compositions of the $Pd_{20}Cu_{40}Ni_{10}P_{20}$ alloy dealloyed in 0.8 mol/L H_2SO_4 + 0.2 mol/L H_3PO_4 solution at 25 ºC for different durations

Dealloying time, s	Pd, at%	Ni, at%	Cu, at%	P, at%
600	38	8	34	20
1800	61	5	21	13
7200	88	1	4	7

The surface morphologies of the samples dealloyed for different durations were observed by SEM and the images are shown in Figure 3. After 600 s of dealloying, nanopores are formed on the sample surface. However, the morphology is not homogeneous. There are less attacked areas pointed

by the white arrow in Figure 3(a) and highly coarsened areas pointed by the black arrow. It might be related to the inhomogeneous chemical compositions on the surface of the as-spun $Pd_{30}Cu_{40}Ni_{10}P_{20}$ metallic glass. Melt-spinning technique will inevitably cause located contamination and oxidation on the ribbon surface. These defects are electrochemically more active than the glassy area. Therefore, quicker leaching will take place in these located areas and coarsening near there is thus fastened [25]. Though the pore size is in a wide range of distribution, the metallic ligaments are relatively homogenous and their width is about 5 nm. The sample dealloyed for 1800 s exhibits a more homogenous structure on the surface. The diameter of the nanopores is ranging within 10~15 nm while the ligament is about 5~6 nm in width. The formation of a more homogenous structure can be attributed to the continuous undercutting of the ligaments which takes place during dealloying. Once the formed ligaments are undercut, fresh surface underneath will be exposured to the electrolyte. Since the inner part of the as-spun $Pd_{30}Cu_{40}Ni_{10}P_{20}$ metallic glass are free of contaminations and oxides, more homogenous nanoporous structure is seen when the dealloying time increases. The longest dealloying duration of 7200 s does not cause significant change in morphology when compared with the sample dealloyed for 1800 s, demonstrating the formation of a highly stable nanoporous structure with small pores. The glassy structure and the multiple components in the precursor alloy are attributed to the hindered Pd diffusion and a slow coarsening rate of the nanoprous structure.

The as-spun $Pd_{30}Cu_{40}Ni_{10}P_{20}$ metallic glass was also dealloyed at different temperatures. The chemical compositions measured by EDS are shown in Table 2. The increase in dealloying temperature leads to the increase in Pd content and dramatic decrease in Cu, Ni and P contents, indicating a much higher corrosion rate (leaching rate) at an elevated temperature.

Table 2. Chemical compositions of the $Pd_{20}Cu_{40}Ni_{10}P_{20}$ alloy dealloyed in 0.8 mol/L H_2SO_4 + 0.2 mol/L H_3PO_4 solution at different temperatures for 7200 s

Dealloying temperature, ºC	Pd, at%	Ni, at%	Cu, at%	P, at%
0	43	8	33	16
25	67	3	20	10
50	85	2	6	7

Figure 4 is the SEM images of the samples dealloyed at 0 ºC, 25 ºC and 50 ºC for 3600 s under an applied potential of 820 mV *vs* SCE. Open interpenetrating spongy-like porous structures can be seen on all these samples. The average pore size of the samples is about 7 nm, 12 nm and 50 nm, respectively. The ligament width also increases with the increasing dealloying temperature (6 nm at 0 ºC, 7 nm at 25 ºC and 14 nm at 50 ºC, respectively). The coarsening of nanoporous structure with the increase in dealloying temperature can be attributed to the enhanced dealloying kinetics. Similar phenomenon has been observed in dealloying AuAg solid solution at temperatures ranging from -20~25 ºC in concentrated HNO_3 [26].

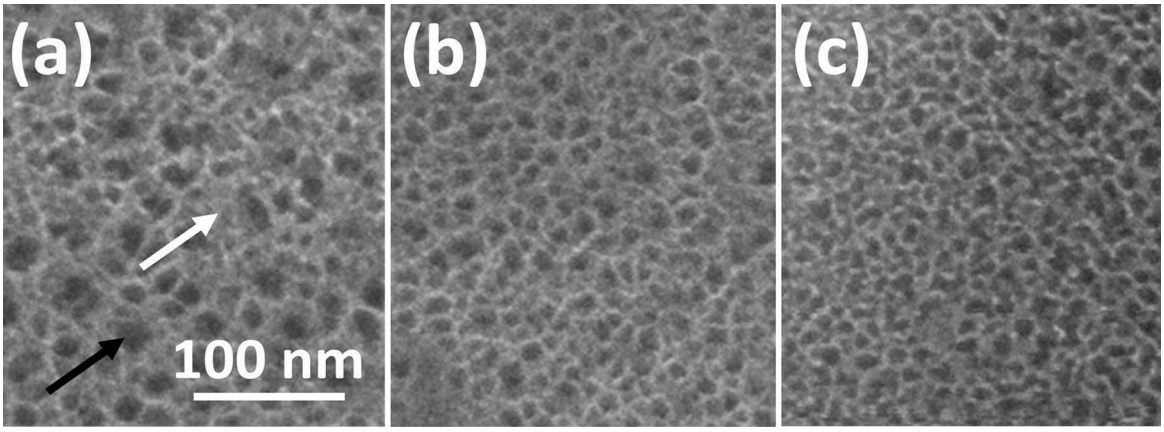

Figure 3. SEM images of the $Pd_{20}Cu_{40}Ni_{10}P_{20}$ alloy dealloyed at 25 ºC for 600 s (a), 1800 s (b) and 7200 s (c)

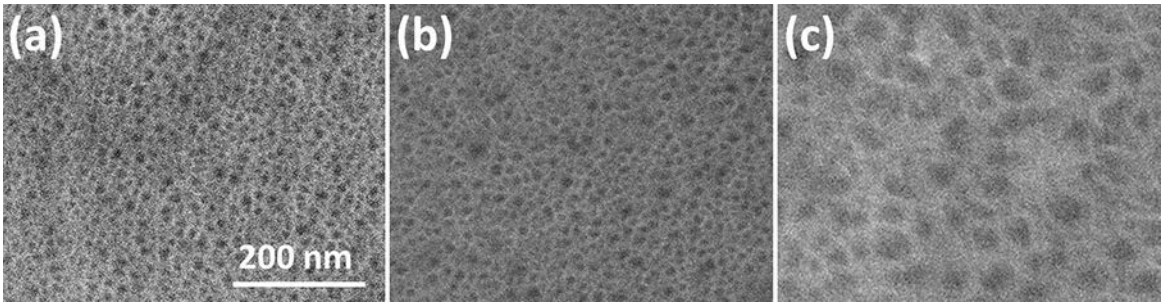

Figure 4. SEM images of the $Pd_{20}Cu_{40}Ni_{10}P_{20}$ alloy dealloyed at 0 ºC (a), 25 ºC (b) and 50 ºC (c) for 3600 s

3.3 Catalytic activities of the dealloyed porous samples

As described above, smaller pore size can be obtained by dealloying at low temperature. To compare the catalytic activity of the porous alloys with different pore size, the fully dealloyed samples (0 ºC dealloyed for 43200 s (EDS: 88 at% Pd, 3 at% Cu, 2 at% Ni, 7 at% P); 25 ºC dealloyed for 7200 s; 50 ºC dealloyed for 3600 s) were selected as catalysts. The EDS analysis already shows that these samples have similar chemical compositions, i.e., Pd~85-88 at%, Cu~3-6 at%, Ni 2-3 at% and P~7-8 at%. However, the average pore/ligament sizes are different, 10 nm/6 nm at 0 ºC, 13 nm/8 nm at 25 ºC and 50 nm/14 nm at 50 ºC, respectively.

Figure 5 shows the cyclic voltammograms (CV) of the fully dealloyed porous samples in a mixed solution of 0.5 M H_2SO_4+0.5 M HCOOH (*vs* RHE) at a scan rate of 50 mV/s. A CV curve of a commercial Pd/C catalyst is also included for comparison. The current densities were normalized by the electrochemically active surface areas of the catalyst, which is calculated by integrating the Pd reduction peak area in 0.5 M H_2SO_4. In the CV curves, the broad peaks in the region between 0mV and 200 mV correspond to the adsorption and desorption of hydrogen and the peak at about 300~600 mV is attributed to the formic acid oxidation [27]. The porous samples dealloyed at 0 ºC and 25 ºC show lower formic acid oxidation potential (300 mV and 345 mV, respectively) when compared to the commercial Pd/C catalyst (490 mV), demonstrating that these two samples have higher catalytic activity. In contrast, the sample dealloyed at 50 ºC exhibits much higher formic acid oxidation potential of 589 mV. Moreover, there is a weak oxidation peak in the potential range of 800-1000 mV, corresponding to indirect oxidation of formic acid. The indirect oxidation will generate CO and poison the catalyst. It is clear that smaller pore size leads to higher catalytic activity in this study. Fujita et al has shown that there are a high density of atomic steps and kinks on the curved surfaces of nanoprous metals, which are active sites for catalytic reaction[28]. Thus, the results are reasonable since smaller pores are always associated with higher curvature change along the surface of the metallic ligaments providing the alloy with more active sites and higher catalytic activity.

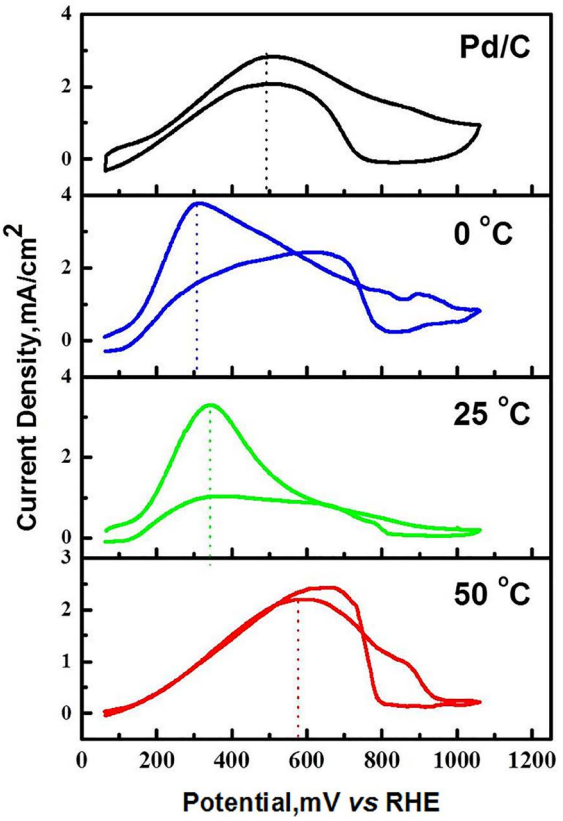

Figure 5. CV curves of the $Pd_{20}Cu_{40}Ni_{10}P_{20}$ alloy fully dealloyed at different temperatures

To further investigate the catalytic stability of the catalyst, chronoamperometry test was performed on the fully dealloyed samples at different temperatures and the results were shown in Figure 6. When compared with the commercial Pd/C catalyst, all the fully dealloyed samples show higher catalytic stability. And the specimen dealloyed at 25ºC displays the best stability as can be evidenced from the highest stable current density and the slowest rate of current reduction. Though the sample dealloyed at 0ºC has the smallest pore size and the best catalytic activity among the dealloyed samples, it exhibit the lowest catalytic stability. The reason might also be related to the small pore size. Porous samples with smaller pores always have higher energy instability which is always associated with faster coarsening. And coarsening will lead to the decrease in catalytic current density.

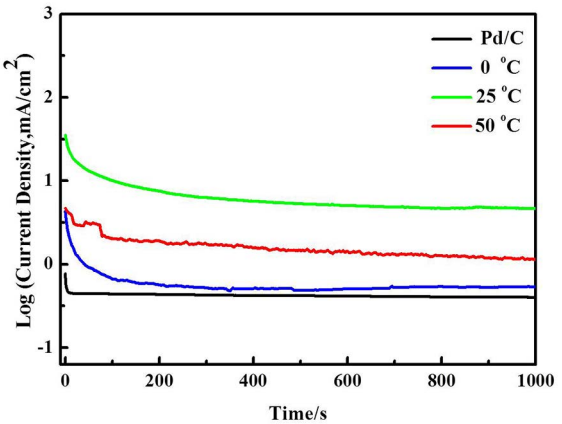

Figure 6. I-t curves of the $Pd_{20}Cu_{40}Ni_{10}P_{20}$ alloy fully dealloyed at different temperatures, the applied potentials are the corresponding peak potentials in CV curves in Figure 5

4. Conclusions

In summary, we have investigated the influence of dealloying time and temperature on the microstructure of the dealloyed $Pd_{30}Cu_{40}Ni_{10}P_{20}$ metallic glass. The results show that the nanoporous structure is highly stable when the dealloying temperature is lower than 25 ºC. Among the fully dealloyed porous samples prepared at different temperate, the one with the smallest pore size of 10 nm exhibit the highest catalytic activity while the specimen with an average pores size of 13 nm shows the highest catalytic stability.

5. Acknowledgments

This work was supported by the Hwa Ying Culture & Education Foundation; the National Science Foundation of China [grant numbers 51771052]; And the Fundamental Research Funds for the Central Universities [grant numbers 2242018K41056].

6. References

1. Zhang JT, Li CM. Nanoporous metals: fabrication strategies and advanced electrochemical applications in catalysis, sensing and energy systems. Chemical Society Reviews. 2012;41(21):7016-7031.

2. Zhang ZH, Wang Y, Qi Z, Zhang WH, Qin JY, Frenzel J. Generalized Fabrication of Nanoporous Metals (Au, Pd, Pt, Ag, and Cu) through Chemical Dealloying. Journal of Physical Chemistry C. 2009;113(29):12629-12636.

3. Kang JL, Hirata A, Qiu HJ, Chen LY, Ge XB, Fujita T, et al. Self-Grown Oxy-Hydroxide@ Nanoporous Metal Electrode for High-Performance Supercapacitors. Advanced Materials. 2014;26(2):269-272.

4. Phan DT, Chung GS. A novel nanoporous Pd-graphene hybrid synthesized by a facile and rapid process for hydrogen detection. Sensors and Actuators B: Chemical. 2015;210:661-668.

5. Lang XY, Han GF, Xiao BB, Gu L, Yang ZZ, Wen Z, et al. Mesostructured Intermetallic Compounds of Platinum and Non-Transition Metals for Enhanced Electrocatalysis of Oxygen Reduction Reaction. Advanced Functional Materials. 2015;25(2):230-237.

6. Zhang XL, Li GJ, Duan D, Wang HY, Sun ZB. Formation and control of nanoporous Pt ribbons by two-step dealloying for methanol electro-oxidation. Corrosion Science. 2018;135:57-66.

7. Erlebacher J, Aziz MJ, Karma A, Dimitrov N, Sieradzki K. Evolution of nanoporosity in dealloying. Nature. 2001;410(6827):450-453.

8. Liu K, Bai YC, Zhang L, Yang ZB, Fan QK, Zheng HQ, et al. Porous Au-Ag Nanospheres with High-Density and Highly Accessible Hotspots for SERS Analysis. Nano Letters. 2016;16(6):3675-3681.

9. Morrish R, Dorame K, Muscat AJ. Formation of nanoporous Au by dealloying AuCu thin films in HNO3. Scripta Materialia. 2011;64(9):856-859.

10. Zhang XM, Li YX, Zhang HW, Liu Y. Evolution of porous structure with dealloying corrosion on Gasar Cu-Mn alloy. Transactions of Nanoferrous Metals Society of China. 2015;25(4):1200-1205.

11. Biener J, Hodge AM, Hayes JR, Volkert CA, Zepeda-Ruiz LA, Hamza AV, et al. Size effects on the Mechanical Behavior of Nanoporous Au. Nano Letters. 2006;6(10):2379-2382.

12. El Mel AA, Boukli-Hacene F, Molina-Luna L, Bouts N, Chauvin A, Thiry D, et al. Unusual dealloying effect in gold/copper alloy thin films: the role of defects and column boundaries in the formation of nanoporous gold. ACS Applied Materials & Interfaces. 2015;7(4):2310-2321.

13. Inoue A, Takeuchi A. Recent progress in bulk glassy, nanoquasicrystalline and nanocrystalline alloys. Materials Science and Engineering: A. 2004;375-377:16-30.

14. Löffler JF. Bulk metallic glasses. Intermetallics. 2003;11(6):529-540.

15. Wang WH, Dong C, Shek CH. Bulk metallic glasses. Materials Science and Engineering: R: Reports. 2004;44(2-3):45-89.

16. Zhou M, Huang X, Hagos K, Cui YW, Ma LQ. Nanoporous copper fabricated from Zr65Cu17.5Fe10Al.7.5 amorphous alloy and its electrocatalytic oxidation performance. Intermetallics. 2017;90:23-29.

17. Thorp JC, Sieradzki K, Tang L, Crozier PA, Misra A, Nastasi M, et al. Formation of nanoporous noble metal thin films by electrochemical dealloying of PtxSi1-x. Applied Physics Letters. 2006;88(3):033110.

18. Yu JS, Ding Y, Xu CX, Inoue A, Sakurai T, Chen MW. Nanoporous Metals by Dealloying Multicomponent Metallic Glasses. Chemistry of Materials. 2008;20(14):4548-4550.

19. Zeng YQ, Yang SC, Xiang H, Dong XZ, Chen LY, Chen MW, et al. Multicomponent nanoporous metals prepared by dealloying Pd80-xNixP20 metallic glasses. Intermetallics. 2015;61:66-71.

20. Lang XY, Guo H, Chen LY, Kudo A, Yu JS, Zhang W, et al. Novel Nanoporous Au-Pd Alloy with High Catalytic Activity and Excellent Electrochemical Stability. Journal of Physical Chemistry C. 2010;114(6):2600-2603.

21. Chen LY, Guo H, Fujita T, Hirata A, Zhang W, Inoue A, et al. Nanoporous PdNi Bimetallic Catalyst with Enhanced Electrocatalytic Performances for Electro-oxidation and Oxygen Reduction Reactions. Advanced Functional Materials. 2011;21(22):4364-4370.

22. Liu AH, Geng HR, Xu CX, Qiu HJ. A three-dimensional hierarchical nanoporous PdCu alloy for enhanced electrocatalysis and biosensing. Analytica Chimica Acta. 2011;703(2):172-178.

23. Zeng YQ, Inoue A, Nishiyama N, Chen MW. Remarkable effect of minor boron doping on the formation of the largest size Ni-rich bulk metallic glasses. Scripta Materialia. 2009;60(11):925-928.

24. Wagner K, Brankovic SR, Dimitrov N, Sieradzki K. Dealloying below the Critical Potential. Journal of the Electrochemical Society. 1997;144(10):3545-3555.

25. Zhang XH, Zeng YQ, Yin L, Jiang JQ, Pan Y, Li R, et al. Formation of micro/nano pits with high catalytic activity on Fe80B20 amorphous alloy. Corrosion Science. 2018;141:109-116.

26. Qian LH, Chen MW. Ultrafine nanoporous gold by low-temperature dealloying and kinetics of nanopore formation. Applied Physics Letters. 2007;91(8):083105.

27. Chen D, Sun PC, Liu H, Yang J. Bimetallic Cu-Pd alloy multipods and their highly electrocatalytic performance for formic acid oxidation and oxygen reduction. Journal of Materials Chemistry A. 2017;5(9):4421-4429.

28. Fujita T, Chen MW. Characteristic Length Scale of Bicontinuous Nanoporous Structure by Fast Fourier Transform. Japanese Journal of Applied Physics. 2008;47(2R):1161-1163.